

Symmetry breaking effects on spin and electronic transport in graphene

Mahmoud M. Asmar* and Sergio E. Ulloa†

*Department of Physics and Astronomy and Nanoscale and Quantum
Phenomena Institute, Ohio University, Athens, Ohio 45701-2979*

The decoration of graphene samples with adatoms or nanoparticles leads to the enhancement of spin-orbit interactions as well as to the introduction of symmetry breaking effects that could have drastic effects on spin and electronic transport phenomena. We present an analysis based on symmetry considerations and examine the impact on the scattering matrix for graphene systems containing defects that enhance spin-orbit interactions, while conserving the electronic total angular momentum. We show that the appearance and dominance of skew scattering, and the related observation of valley and/or spin Hall effect in decorated graphene samples, suggests the set of symmetries that adatom perturbations should satisfy. We further show that detailed measurements of the transport and elastic times as function of carrier concentration make it possible to not only extract the strength of the spin-orbit interaction, as suggested before, but also obtain the amplitude of the symmetry breaking terms introduced. To examine how different terms would affect measurements, we also present calculations for typical random distributions of impurities with different perturbations, illustrating the detailed energy dependence of different observables.

PACS numbers: 72.10.Fk, 75.76.+j, 72.80.Vp, 03.65.Pm

I. INTRODUCTION.

The low energy Dirac fermions residing near the corners of the Brillouin zone on the honeycomb lattice of graphene¹ have inspired the theoretical prediction and subsequent experimental realization of a variety of new two-dimensional materials^{2,3} and novel electronic phases of matter in two and three dimensions.⁴⁻⁷ The ability to manipulate and control the electronic and spin properties of graphene and related materials by decoration,⁸⁻¹¹ stacking,^{12,13} intercalation¹⁴⁻¹⁸ and distortion¹⁹⁻²⁷ may also lead to important technological advances.

The helical nature of the massless Dirac particles in pristine graphene gives rise to interesting phenomena, such as Klein tunneling,²⁸ and the observation of weak anti-localization in this material.²⁹ However, it has been shown that the transport properties of graphene strongly depend on the nature, symmetries and concentration of the impurities present in typical samples.²⁹⁻⁴⁰ Deformations from impurities may belong to different symmetry classes. As such, they could either enhance or weaken the signatures expected from the chiral nature of the scatterers of graphene and drastically modify the electronic and spin transport properties.

An interesting example of interactions protected by lattice symmetries is provided by the appearance of a spin orbit interaction (SOI) that preserves all symmetries of the honeycomb lattice,² and leads to the formation of topologically protected edge states—anticipating the existence of topological insulating materials.³ In contrast, an electric field perpendicular to a graphene sample leads to inversion ($z \rightarrow -z$) symmetry breaking, allowing the appearance of a Bychkov-Rashba SOI.^{2,41} The small atomic number of carbon makes an intrinsic SOI small (a few μeV),⁴² while the Rashba SOI has strength of hundreds of μeV for typical values of electric fields.⁴²

Methods that rely on the artificial functionalization

of graphene could lead to sizable enhancement of SOIs. Successful examples of these methods include the intercalation of gold atoms between graphene and the Ni substrate,¹⁴⁻¹⁶ weak hydrogenation,^{8,9} and the deposition of large copper or gold nanoparticles.¹¹ Other approaches are also promising, including externally induced curvature of samples,^{19,22,25} decoration with heavy adatoms such as thallium and indium,^{43,44} and the deposition of graphene on the surface of a strong topological material.¹⁷ These methods have achieved or project the enhancement of SOI of up to several tens of meV, leading to clear measurable effects on the electron dynamics.^{8,10,40,45-48}

The methods used to enhance SOIs in graphene require the presence of adatoms or local defects/deformations that accommodate on the graphene lattice in different ways. These perturbations introduce additional effects from the lattice symmetries they may break. The enhancement of intrinsic and/or Rashba SOIs on the dynamics of electrons in graphene has been analyzed for the most part in the framework of a single-valley Dirac description.^{8,10,45,49} In that limit—valid for potential scatterers with large characteristic spatial variation compared to the lattice constant—the scattering preserves helicity, it is predominantly forward, and gives rise to Klein-tunneling, as mentioned above.^{35,36,45} If the scattering centers lead to enhancement of Rashba and/or intrinsic SOIs, the electronic scattering has been shown to become increasingly isotropic.⁴⁵ This scattering could also lead to spin Hall effect via enhanced skew scattering close to the resonant regime.⁹⁻¹¹

Here, going beyond the single-valley Dirac treatment,⁴⁵ we study the scattering properties of Dirac fermions from adatoms or imperfections on graphene, as they may lead to the reduction of lattice symmetries. Through a symmetry analysis and considering intra- and intervalley processes, we are able to

identify the constants of motion for different situations. We further examine the constraints imposed by these conserved quantities on the scattering matrix and the observable consequences in transport experiments.

We focus in particular on the ratio of transport to elastic times, $\xi = \tau_{tr}/\tau_e$, and its dependence on carrier concentration, which was previously studied for systems where SOIs were locally enhanced, and no additional local symmetry breaking effects were considered.⁴⁵ We find that this ratio depends strongly on the microscopic potential perturbations, which make ξ deviate from its characteristic low-energy value of 2.⁴⁵ This deviation depends on the carrier concentration and strength of the symmetry breaking, as well as on the local potential shift produced by the impurities. As backscattering becomes stronger, the ratio takes a value closer to 1 (the limit for massive Schrödinger particles). We further study the effects symmetry breaking perturbations may produce on the detection of Rashba and intrinsic SOIs. The dependence of ξ on carrier concentration in the presence of Rashba SOI is shown to be *qualitatively* different for different symmetry breaking terms in the perturbation. Systematic experimental studies of ξ in given graphene systems would allow the identification and simultaneous evaluation of the relative strengths of the different perturbations. Finally, from the symmetries of the scattering matrix, we show which systems may display non-zero valley and/or spin transport skewness (skew scattering). In particular, we find that disorder that is not invariant under “effective time reversal” leads to a reduction of spin skew scattering, due to the enhancement of valley skew scattering; this allows one to identify what kind of decorated system will display skew scattering and may result in the appearance of valley and/or spin Hall effect.

We further illustrate the impact of the symmetry considerations described above for typical graphene samples. Throughout the discussion of the different perturbations, we present numerical results for the anticipated dependence of ξ and skewness to different effects, by analyzing the results for a random impurity distribution. This allows us to gain insights into the contribution of different effects to various measurable quantities.

The remainder of the paper considers the symmetries of different perturbation terms, especially their invariance under time reversal, and the consequences of these symmetries on the corresponding scattering matrix in the problem. In Sec. II A we consider the spinless case, and study the scattering matrix and scattering amplitudes, as well as their impact in transport and elastic times. In Sec. II B we include the spin degree of freedom and associated spin-orbit interaction terms, while Sec. II C studies the consequences on skew scattering. A general discussion of the results in Sec. III is followed by conclusions in Sec. IV.

II. SYMMETRY OF PERTURBATIONS IN GRAPHENE

A. Spinless scattering

In order to analyze the effects of symmetry breaking on the dynamics of Dirac fermions in graphene, we first consider the Hamiltonian

$$H = H_0 + V_T, \quad (1)$$

where

$$H_0 = v_F \vec{\alpha} \cdot \vec{k}, \quad (2)$$

($\hbar = 1$ and $\vec{k} = (k_x, k_y)$) is the pristine graphene Hamiltonian, represented in the four-dimensional chiral basis $\psi = (\psi_{A,K}, \psi_{B,K}, \psi_{B,K'}, \psi_{A,K'})^T$, with

$$\alpha_i = \tau_3 \otimes \sigma_i = \begin{pmatrix} \sigma_i & 0 \\ 0 & -\sigma_i \end{pmatrix}, \quad (3)$$

($i = 1, 2, 3$), where σ_i and τ_i are a set of Pauli matrices that act on the sublattice index (A, B) and the valley index (K, K'), respectively. It is also useful to define

$$I = \sigma_0 \otimes \tau_0 = \begin{pmatrix} \sigma_0 & 0 \\ 0 & \sigma_0 \end{pmatrix}, \quad (4)$$

$$\gamma^5 = \tau_3 \otimes \sigma_0 = \begin{pmatrix} \sigma_0 & 0 \\ 0 & -\sigma_0 \end{pmatrix}, \quad (5)$$

and

$$\beta = \tau_1 \otimes \sigma_0 = \begin{pmatrix} 0 & \tau_0 \\ \tau_0 & 0 \end{pmatrix}. \quad (6)$$

As in the case of the three dimensional Dirac equation,^{50,51} these matrices satisfy

$$\{\alpha_i, \alpha_j\} = 2\delta_{i,j}, \quad (7)$$

$$[\alpha_i, \gamma^5] = 0, \quad (8)$$

$$\{\alpha_i, \beta\} = 0, \quad (9)$$

and

$$\{\gamma^5, \beta\} = 0. \quad (10)$$

1. Symmetry considerations.

Here we define, V_T , as the set of time reversal invariant perturbations,^{30,32,33,37}

$$[V_T, \mathcal{T}] = 0, \quad (11)$$

where

$$\mathcal{T} = \beta \gamma^5 \alpha_1 \mathcal{C} \quad (12)$$

is the time reversal operator, $\mathcal{T}^2 = 1$, and \mathcal{C} is the anti-linear complex conjugation operator.^{45,52,53} Additionally, the helicity operator

$$\hat{h} = \gamma^5 \vec{\alpha} \cdot \vec{k}/k, \quad (13)$$

(with $k = |\vec{k}|$) indicates the pseudo-spin projection in the direction of momentum,^{50,52} with

$$[H_0, \hat{h}] = 0, \quad (14)$$

and

$$\{\mathcal{T}, \hat{h}\} = 0. \quad (15)$$

The conservation of total angular momentum in a system in which perturbations V_T are present requires

$$[H, J_z] = 0, \quad (16)$$

where

$$J_z = -i\partial_\theta + \frac{1}{2}\gamma^5\alpha_3. \quad (17)$$

In systems where the spatial dependence of the perturbations has circular symmetry, such as the simple form $H = H_0 + V_T\Theta(R-r)$, there exist a subset of time reversal invariant interactions that conserve the total angular momentum,

$$V_{T,J} \subset V_T. \quad (18)$$

This set can be shown to be composed of the elements^{23,26,27,30-34,37-39,52}

$$V_{T,J} = \{vI, s\alpha_3, t\beta e^{i\gamma^5\phi}\}, \quad (19)$$

where v , s , t and ϕ are real parameters. Notice that with the exception of vI , the $V_{T,J}$ terms anticommute with α_1 and α_2 , so that they generate gaps in the spectrum and are referred to as ‘‘massive terms’’.⁵² The v term describes a constant local potential shift caused by the adatoms, while the s term describes a staggered potential effect some perturbations may add, where the A and B sites are affected differently. The t terms describe a hopping modulation amplitude caused by the adatoms/defects, where ϕ describes the angle of dimerization of the resulting deformation, as in a Kekulé pattern.^{23,27,52}

One can also define the subset

$$V_{T,J,h} \subset V_{T,J}, \quad (20)$$

for perturbations that in addition to commuting with \mathcal{T} and J_z , also commute with the helicity operator \hat{h} , and find that

$$V_{T,J,h} = \{vI, t\beta e^{i\gamma^5\phi}\}. \quad (21)$$

In these cases the eigenstates of the Hamiltonian,

$$H = H_0 + V_{T,J,h}, \quad (22)$$

can be identified by corresponding quantum numbers, such that

$$\hat{h}\psi_{\pm,j} = \pm\psi_{\pm,j} \quad (23)$$

(as $\hat{h}^2 = 1$), and

$$J_z\psi_{\pm,j} = j\psi_{\pm,j}, \quad (24)$$

where j is half-integer. One can also find an additional operator

$$\mathcal{T}_1 = ie^{-i\gamma^5\phi}\gamma^5\alpha_2\mathcal{C}, \quad (25)$$

such that $\mathcal{T}_1^2 = -1$,

$$[\mathcal{T}_1, H] = [\mathcal{T}_1, \hat{h}] = 0, \quad (26)$$

while

$$\{\mathcal{T}_1, J_z\} = 0. \quad (27)$$

\mathcal{T}_1 can be seen as a combination of a chiral rotation and the effective time reversal operator in each Dirac point.⁵²⁻⁵⁵ This operator together with the time reversal operator \mathcal{T} , relate the states with angular momentum j and $-j$, which can be chosen such that

$$\mathcal{T}_1\psi_{\pm,j} = \pm(-1)^j\psi_{\pm,-j}, \quad (28)$$

and

$$\mathcal{T}\psi_{\pm,j} = \mp(-1)^{j+\frac{1}{2}}\psi_{\mp,-j} \quad (29)$$

(see appendix A).

2. Symmetry constraints on scattering and electronic transport.

Conservation of total angular momentum allows one to use the j block-diagonal character of the scattering matrix. The lack of valley mixing in the area outside the potential perturbation region, $r > R$, enables the determination of the scattering amplitudes between the $+$ and $-$ (or correspondingly K and K') states for each j block. The components of each 4×4 block (\hat{S}_j) are given by

$$\hat{S}_{j,\tau\tau'} = S_{j,\tau\tau'}\sigma_0, \quad (30)$$

where $\tau, \tau' = \pm$. Unitarity of \hat{S} requires

$$\hat{S}_j\hat{S}_j^\dagger = I, \quad (31)$$

and symmetry under operators \mathcal{T}_1 and \mathcal{T} determine relations between the j and $-j$ blocks, such that

$$\gamma^5\mathcal{T}_1S_j\mathcal{T}_1^{-1}\gamma^5 = S_{-j}^\dagger \quad (32)$$

and

$$\gamma^5\mathcal{T}S_j\mathcal{T}^{-1}\gamma^5 = S_{-j}^\dagger \quad (33)$$

(see appendix A). These relations have important consequences on the possible scattering processes (see Eq. A13 in appendix), which allow us to obtain different scattering functions.

For example, the differential cross section $\sigma(\theta)$ contains information on the angular distribution of the scattering. From the relations in Eq. A13, one can determine the angular dependence of the differential cross section in terms of the j -scattering amplitudes. For a circularly symmetric region where

$$H = H_0 + V_{T,J,h} \quad (34)$$

for $r < R$, and

$$H = H_0 \quad (35)$$

for $r > R$, we have

$$\begin{aligned} \sigma_{\tau\tau}(\theta) &= \frac{2}{\pi k} \left| \sum_{j \geq \frac{1}{2}}^{\infty} f_{\tau\tau,j} \cos j\theta \right|^2 \\ \sigma_{\tau\bar{\tau}}(\theta) &= \frac{2}{\pi k} \left| \sum_{j \geq \frac{1}{2}}^{\infty} f_{\tau\bar{\tau},j} \sin j\theta \right|^2 \\ \sigma(\theta) &= \sum_{\tau,\tau'} \sigma_{\tau\tau'}(\theta), \end{aligned} \quad (36)$$

where $f_{\tau\tau',j}$ are the scattering amplitudes defined in appendix B, and $\bar{\tau} = -\tau$. Notice that the differential cross sections for valley-preserving processes, $\sigma_{\tau\tau}(\theta)$, display a maximum at $\theta = 0$, and vanish at $\theta = \pi$ (which signals the absence of backscattering). The situation is reversed for the valley-flipping cross sections, $\sigma_{\tau\bar{\tau}}$, which display a maximum at $\theta = \pi$, and vanish at $\theta = 0$. It is then clear that any backscattering in the system is caused solely by valley flipping events.

The scattering matrix elements are naturally related to experimentally measurable quantities via the total, transport and skew cross sections defined in appendix B. The *transport* cross section σ_{tr} is related to the transport time

$$\tau_{tr}^{-1} = n_{imp} v_F \sigma_{tr}, \quad (37)$$

and the *total* cross section σ_t to the elastic scattering time

$$\tau_e^{-1} = n_{imp} v_F \sigma_t, \quad (38)$$

where n_{imp} is the impurity concentration. The ratio

$$\xi = \frac{\tau_{tr}}{\tau_e} = \frac{\sigma_t}{\sigma_{tr}} \quad (39)$$

reflects the degree of angular isotropy in the scattering processes,^{35,36,45} with $\xi = 1$ in the fully isotropic (massive) limit at low energies. The *skew* cross section σ_{sk} , quantifies the asymmetry of the scattering about the electron's direction of incidence, and it is related to the appearance of Hall currents, as characterized through the skew parameter¹⁰

$$\gamma = \frac{\tau_{tr}}{\tau_{sk}} = \frac{\sigma_{sk}}{\sigma_{tr}}. \quad (40)$$

The form of the differential cross section in Eq. 36 results in no skewness, since it is symmetric about the x -axis ($\theta = 0$), yielding null skew cross sections (see appendix B).

The ratio of scattering times,

$$\xi = \frac{\sum_{\tau\tau'} \sigma_{t,\tau\tau'}}{\sum_{tr,\tau\tau'} \sigma_{\tau\tau'}}, \quad (41)$$

can be determined analytically in the low energy regime $kR \ll 1$, where the only contributing channels to the scattering are the two lowest, $j = \pm \frac{1}{2}$.⁵⁴ Using the relations in Eq. B10, one gets

$$\xi = \frac{\tau_{tr}}{\tau_e} \simeq \frac{2 \left(|f_{++,\frac{1}{2}}|^2 + |f_{+-,\frac{1}{2}}|^2 \right)}{|f_{++,\frac{1}{2}}|^2 + 3|f_{+-,\frac{1}{2}}|^2}. \quad (42)$$

Remote charge impurities lead to a local change in the carrier concentration in their area of influence and a local change of the Fermi momentum in that region. These impurities can then be described in the continuum model by the perturbation vI , which respects all the symmetries of the graphene lattice and belongs to the A_1 representation of the C_{6v} point group.^{30,39} This shift does not lead to valley mixing and from Eq. 42 (as $f_{\tau\bar{\tau},\frac{1}{2}} = 0$) one finds $\xi = 2$ for $kR \ll 1$, regardless of the value of v , as has been experimentally shown.^{35,36} This is a direct consequence and signature of the anisotropy and predominant forward scattering in graphene.

Some impurities may generate a staggered potential that differentiates between the A and B sites, as mentioned above, with a perturbation described by $s\alpha_3$ in the continuum model. This term reduces the point symmetries of the lattice (belongs to the B_2 representation of C_{6v}), and although it does not mix valleys, it opens a gap. Moreover, a staggered potential does not commute with \hat{h} or \mathcal{T}_1 , reducing the set of constraints on the scattering matrix (see Eq. B12), to those from time reversal and unitarity. This situation leads to qualitative changes in the isotropy of the scattering process. The presence of $s \neq 0$ not only affects the ratio of scattering times ξ , but also results in a non-zero skew cross section (Eq. B14), given that

$$\sigma_{sk,\tau\tau} = -\sigma_{sk,\bar{\tau}\bar{\tau}} \quad (43)$$

and

$$\sigma_{sk,\tau\bar{\tau}} = 0, \quad (44)$$

and the corresponding appearance of a valley Hall effect.⁵⁶ This effect is associated with the appearance of transverse valley currents, which can be characterized by a valley Hall angle

$$\Theta_{VH} = \frac{j_{VH}}{j_x}. \quad (45)$$

At zero temperature the valley Hall angle is equal to the valley skewness, in the absence of side-jump effects (see

appendix B),

$$\gamma_V = \frac{1}{2}(\gamma_K - \gamma_{K'}) . \quad (46)$$

This effect is found to be robust to a non-zero t valley-mixing perturbation. Note that in the case of valley polarized incident currents, $\gamma = \gamma_V$, leading to the appearance of Hall voltages due to the accumulation of charge on the sample edges.

For impurities that accommodate on the center of the hexagon, as is the case of Ca and Al atoms,²⁴ for a substrate with a periodicity commensurate with graphene,³⁴ and for ‘Kekulé’ distortions with zero dimerization angle,³⁴ the perturbation terms can be described by $Re(t\beta e^{i\gamma^5\phi}) \simeq t\beta$; this does not break point symmetries of graphene (belongs to the A_1 representation of $C_{6\nu}$) but breaks translational invariance, which leads to vanishing Dirac points and the opening of a gap.³⁴ Other hexagon-centered impurities,^{23,24,52} lead to more general perturbations with $\phi \neq 0$, as described by $t\beta e^{i\gamma^5\phi}$ (in the B_1 representation of $C_{6\nu}$), which also open a gap in the spectrum. The presence of these interactions is reflected in particular through the deviation of ξ away from 2 at low energies, as we will describe in detail below.

In the presence of t and s perturbations, ξ not only depends on these parameters but also on the value of v . Since $\{\alpha_3, \beta e^{i\gamma^5\phi}\} = 0$, and as α_i, β , and γ^5 are self-inverse (involutory), and obey $\{\beta, \alpha_i\} = \{\alpha_3, \alpha_i\} = 0$, the local spectrum shows a gap of 2Δ ,

$$k = \sqrt{(E - v)^2 - \Delta^2} , \quad (47)$$

where

$$\Delta^2 = s^2 + t^2 . \quad (48)$$

When the potential shift generated by the impurity is such that $|E - v| \gg |\Delta|$, one recovers the linear (ultra-relativistic regime), $k \approx |E - v| + \mathcal{O}(\Delta^2/|E - v|)$, and the effect of Δ is minimal on the scattering amplitudes; this leads to $f_{\tau\bar{\tau}, \pm\frac{1}{2}} \approx 0$, as well as to $f_{\tau\tau, \frac{1}{2}} \approx f_{\tau\tau, -\frac{1}{2}}$, and consequently $\xi \approx 2$, even when s and t may be nonzero. Δ should then be comparable to the local kinetic energy, $\Delta \approx |E - v|$, in order to have a noticeable effect. In this limit the valley-flipping contributions are non negligible, with $f_{\tau\tau, \frac{1}{2}} \neq f_{\tau\tau, -\frac{1}{2}}$, and the ratio ξ exhibits a large drop at low carrier concentrations, as can be seen in Fig. 1a.

It should be noted that although the ratio ξ has similar dependence on energy in the presence of s or t , the mechanisms by which the scattering isotropy is enhanced are different. In the presence of $t\beta e^{i\gamma^5\phi}$, the isotropy is achieved through valley-flip processes that acquire an amplitude comparable to the valley preserving processes as $|t|/|E - v| \rightarrow 1$, leading to $\xi \approx 1$ in Eq. 42. In the case of the staggered perturbation, the isotropy is enhanced by the decay in amplitude of one of the two available scattering channels (e.g. $f_{\tau\tau, \frac{1}{2}} \rightarrow 0$ while $f_{\tau\tau, -\frac{1}{2}} \neq 0$ at the K point) as $|s|/|E - v| \rightarrow 1$, at each valley independently.⁴⁵

It is then clear that as graphene is perturbed by adatoms or deformations, and different symmetry breaking terms appear in the Hamiltonian, many of the dynamical electronic properties will change depending on details of the specific terms. In particular, the ratio ξ will generically deviate from its value of 2 as the massless nature of free graphene quasiparticles is affected by these perturbations. The appearance of backscattering becomes increasingly important for stronger perturbations and can be detected by different transport measurements.

B. Spin-orbit interactions

In the presence of spin-orbit interactions (SOIs) we consider an extended representation $\psi = (\psi_{A,K,\uparrow}, \psi_{B,K,\uparrow}, \psi_{B,K',\uparrow}, \psi_{A,K',\uparrow}, \psi_{A,K,\downarrow}, \psi_{B,K,\downarrow}, \psi_{B,K',\downarrow}, \psi_{A,K',\downarrow})^T$, and define the corresponding matrices

$$\mathcal{A}_i = \alpha_i \otimes s_0 = \begin{pmatrix} \alpha_i & 0 \\ 0 & \alpha_i \end{pmatrix} , \quad (49)$$

$$\mathcal{B} = \beta \otimes s_0 = \begin{pmatrix} \beta & 0 \\ 0 & \beta \end{pmatrix} , \quad (50)$$

$$\Gamma^5 = \gamma^5 \otimes s_0 = \begin{pmatrix} \gamma^5 & 0 \\ 0 & \gamma^5 \end{pmatrix} , \quad (51)$$

which operate on the pseudospin and valley degrees of freedom, but leave the spin unchanged, as s_0 is the identity in spin space. These operators satisfy

$$\{\mathcal{A}_i, \mathcal{A}_j\} = 2i\delta_{ij} , \quad (52)$$

$$\{\mathcal{B}, \mathcal{A}_i\} = 0 , \quad (53)$$

$$[\mathcal{A}_i, \Gamma^5] = 0 , \quad (54)$$

and

$$\{\mathcal{B}, \Gamma^5\} = 0 . \quad (55)$$

We also define

$$S_i = s_i \otimes \sigma_0 \otimes \tau_0 , \quad (56)$$

which act on the spin degree of freedom, with

$$\{S_i, S_j\} = 2\delta_{ij} , \quad (57)$$

and commute with $\mathcal{A}_i, \mathcal{B}$ and Γ^5 . In this representation, the time reversal,⁵⁷ helicity operator, and total angular momentum are defined as

$$\mathcal{T} = iB\Gamma^5\mathcal{A}_1S_2\mathcal{C} , \quad (58)$$

$$\hat{h} = \Gamma^5\vec{\mathcal{A}} \cdot \vec{k}/k , \quad (59)$$

$$J_z = -i\hbar\partial_\theta + \Gamma^5\mathcal{A}_3/2 + S_3/2 , \quad (60)$$

with J_z having integer eigenvalues, $\mathcal{T}^2 = -1$, and $\{\mathcal{T}, J_z\} = 0$. Similarly, one can define

$$\mathcal{T}_1 = e^{-i\Gamma^5\phi}\Gamma^5\mathcal{A}_2S_2\mathcal{C} , \quad (61)$$

with $\mathcal{T}_1^2 = 1$, and satisfying

$$\{\mathcal{T}_1, J_z\} = 0 . \quad (62)$$

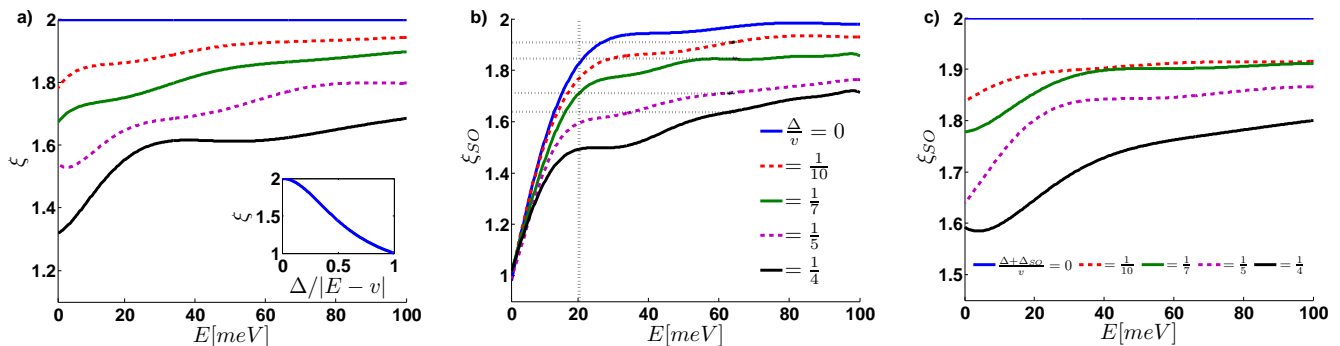


FIG. 1. Numerical calculation of the transport to elastic time ratio ξ (ξ_{SO} in the presence of SOIs), for a set of 500 randomly sized impurities, where ($5 \leq R \leq 15$)Å, and $v = 2\text{eV}$, for the following systems: a) In the presence of symmetry breaking effects described by t and s , notice ξ deviates from the value of 2 by nearly a constant value at large energies, and reaches its minimum at/near zero energy. Inset: Dependence of ξ on $\Delta = \sqrt{t^2 + s^2}$ for fixed values of v and $E = 60\text{meV}$. b) Effects of t and s on ξ_{SO} in the presence of a Rashba interaction $\lambda_R = 20\text{meV}$. Notice the sharp drop of ξ_{SO} at $E \rightarrow 0$ due to the Rashba interaction. The deviation from 2 at high energies is due to t and s , allowing the quantification of their amplitudes. Horizontal dashed lines correspond to the value ξ_{SO} for given t and s in the inset of a); the vertical dashed line shows the value of λ_R ; ξ_{SO} drops rapidly for $E < \lambda_R$. c) Effects of t and s on ξ_{SO} in the presence of intrinsic SOI, $\Delta_{SO} = v/10$. Notice that ξ_{SO} has a similar behavior as in a), indicating that the simultaneous extraction of intrinsic SOI and the symmetry breaking amplitudes t and s from ξ_{SO} is not feasible.

1. Symmetry considerations and constraints on spin transport

In this representation, the set of spin dependent interactions that conserve total angular momentum is found to be

$$V_{T,J}^{SO} = \{ \lambda_R (\mathcal{A}_1 S_2 - \mathcal{A}_2 S_1), \lambda (\mathcal{A}_2 S_2 + \mathcal{A}_1 S_1), \Delta_{SO} \Gamma^5 \mathcal{A}_3 S_3, \Delta_S \Gamma^5 S_3 \}, \quad (63)$$

all with real coefficients. These interactions commute with both \mathcal{T} and \mathcal{T}_1 . For

$$H = H_0 + V_{\mathcal{T}_1}, \quad (64)$$

where

$$V_{\mathcal{T}_1} = V_{T,J}^{SO} \cup \{ vI, t\mathcal{B}e^{i\Gamma^5 \phi} \}, \quad (65)$$

one finds

$$[\mathcal{T}_1, H] = [\mathcal{T}, H] = 0, \quad (66)$$

and utilizing the unitarity of the S matrix one obtains the condition

$$\Gamma^5 \mathcal{T}_1 S_j \mathcal{T}_1^{-1} \Gamma^5 = S_{-j}^\dagger \quad (67)$$

(see Eq. C5).

It should be noted that the SO terms λ_R and λ do *not* lead to a gap opening; instead they break the spin degeneracy by doubling the bands for a fixed energy, such that

$$k_{\pm} = \sqrt{(E - v)^2 \pm 2\Upsilon(E - v)}, \quad (68)$$

where

$$\Upsilon = \sqrt{\lambda_R^2 + \lambda^2}. \quad (69)$$

These interactions split the low energy resonant peaks corresponding to $j = 0$ and $j = \pm 1$ channels whenever $\Upsilon > 2E$,⁴⁵ and produce a noticeable drop at low carrier concentrations ($E < \Upsilon$) in the ratio of cross sections,

$$\xi_{SO} = \frac{\sum_{\tau\tau's's'} t, \sigma_{\tau\tau's's'}}{\sum_{\tau\tau's's'} \sigma_{tr,\tau\tau's's'}}, \quad (70)$$

as shown in Fig. 1b.

The spin independent terms lead also to a variation of ξ_{SO} at low energies, although with a different dependence on the carrier concentration, as shown in Fig. 1a. Therefore, in the presence of λ_R , λ , t and s terms one can determine the value of v and the ratio Δ/v from the behavior of ξ_{SO} with Fermi energy, as illustrated in Fig. 1b.

The intrinsic SOI (Δ_{SO}) does not commute with \mathcal{T}_1 and does not cause spin flips, but opens a gap, and leads to a reduction of ξ_{SO} , such that $\xi_{SO} \rightarrow 1$ as $\Delta_{SO}/|E - v| \rightarrow 1$. However, the gap generated by Δ_{SO} is incompatible with the gaps generated by t and s , since these interactions do not anticommute with the intrinsic SOI.⁵² In this case, the effect of the intrinsic SOI can not be distinguished from symmetry breaking effects in samples through measurements of the ratio ξ_{SO} . In the presence of Δ_{SO} and with no symmetry breaking terms ($t = s = 0$), the dependence of $\xi_{SO}(E)$ on the different values of Δ_{SO} are qualitatively similar to those in Fig. 1a. It is the case that the simultaneous presence of Δ_{SO} , t and s will lead an overestimation of Δ_{SO} from ξ_{SO} measurements, due to the similar deviation caused by t and s , as shown in Fig. 1c.

C. Skew scattering and spin Hall effect

An alternative method to measure the strength of SOIs in graphene was introduced recently by Ferreira *et al.*¹⁰ The method exploits the skew character of scattering in the presence of locally enhanced SOIs. Here, we study effects produced by dimerization perturbations such as $t\mathcal{B}e^{i\Gamma^5\phi}$, and staggered sublattice symmetry breaking, and how they influence skew scattering and the possible determination of the SOI parameters from transport experiments.

In the absence of valley mixing effects or sublattice symmetry breaking, the $V_{T,J}^{SO}$ perturbations commute with both \mathcal{T} and \mathcal{T}_1 , as mentioned above. The symmetries of the scattering matrix result in $\sigma_{sk,\tau\tau\uparrow\uparrow} = -\sigma_{sk,\tau\tau\downarrow\downarrow}$ and $\sigma_{sk,\tau\tau\uparrow\downarrow} = -\sigma_{sk,\tau\tau\downarrow\uparrow} = 0$ (see appendix C). This indicates that carriers with opposite spin are scattered in opposite directions, which would lead to their accumulation on the sample edges and the appearance of a spin Hall effect (SHE) signal.¹⁰

One way to quantify this effect is through the ratio of the skew to transport cross section for each spin projection, γ_\uparrow and γ_\downarrow , and define the spin transport skewness as

$$\gamma_S = \frac{1}{2}(\gamma_\uparrow - \gamma_\downarrow) \quad (71)$$

where

$$\gamma_s = \frac{\sum_{\tau\tau's'} \sigma_{sk,\tau\tau',s's}}{\sum_{\tau\tau's'} \sigma_{tr,\tau\tau',s's}}, \quad (72)$$

(see Eq. C11 in appendix), and γ_S considers valley and spin preserving events, as well as valley and spin reversals. The spin skewness γ_S considers then all processes resulting in spin asymmetries, it is enhanced through resonant scattering, and fully characterizes the spin Hall angle at zero temperature,

$$\theta_{SH} = \left. \frac{j_{SH}}{j_x} \right|_{T=0} = \gamma_S, \quad (73)$$

in the absence of side-jump effects.¹⁰ In the absence of valley mixing or sublattice symmetry breaking, the skew parameters for each spin are equal in magnitude and opposite in sign, leading to $\gamma_S = \gamma_\uparrow$. This effect was recently observed in graphene samples in which the SO was enhanced through the deposition of large copper or gold nanoparticles,¹¹ and in weakly hydrogenated samples, and found to yield rather strong SHE signals.⁹

In the presence of valley mixing, $t\mathcal{B}e^{i\Gamma^5\phi}$, in addition to SOI terms, both \mathcal{T} and \mathcal{T}_1 commute with the Hamiltonian, resulting in the following relations, $\sigma_{sk,\tau\tau,ss} = -\sigma_{sk,\tau\tau,\bar{s}\bar{s}} = -\sigma_{sk,\bar{\tau}\bar{\tau},\bar{s}\bar{s}} = \sigma_{sk,\bar{\tau}\bar{\tau},ss}$ and $\sigma_{sk,\tau\tau',s\bar{s}} = \sigma_{sk,\tau\tau',\bar{s}s} = 0$, as well as a nonzero value of the skew parameter γ ; its dependence on t as a function of carrier concentration is illustrated in Fig. 2a.

However, in the presence of a staggered perturbation $s\mathcal{A}_3$, the Hamiltonian does not commute with the operator \mathcal{T}_1 . This reduces the set of conditions imposed on the

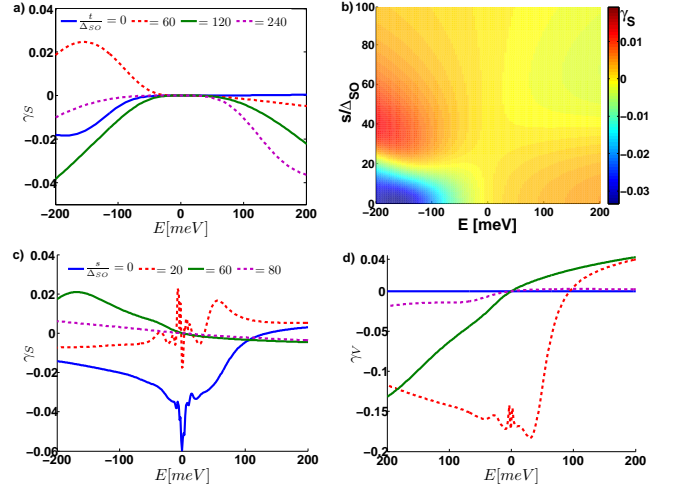


FIG. 2. a) Spin skew parameter γ_S as function of energy for different values of t in a system with $\Delta_{SO} = 25\text{meV}$, $v = 2\text{eV}$ and $R = 6\text{\AA}$. Even for large values of t the skew scattering persists, as expected from symmetry arguments. b) Map of spin skew parameter γ_S vs symmetry breaking staggered interaction s and energy (carrier concentration) E , for Δ_{SO} , v and R as in a). Notice that for large values of s the skew parameter $\gamma \rightarrow 0$, showing that skew scattering is not robust to this kind of perturbation. c) Spin skew parameter dependence on s for a set of 2000 randomly sized impurities ($3 \leq R \leq 9\text{\AA}$), for values of v and Δ_{SO} as in (a). This shows the robustness of skew scattering to random impurity size, but not under s perturbations. d) Valley skew parameter dependence on s for the same set of random impurities and s values in (c). Note that in systems with $s > \Delta_{SO}$, it is generally the case that $|\gamma_V| > |\gamma_S|$ (notice different vertical scales). Both γ_S and γ_V vanish away from the resonant regime, as it is the case for $s/\Delta_{SO} = 80$.

skew cross section elements, so that the relation between $\sigma_{sk,\tau\tau,ss}$ and $\sigma_{sk,\tau\tau,\bar{s}\bar{s}}$ depends on the staggered parameter s (see Eqs. C14 and C11). A nonzero s leads to a reduction of γ_S and the corresponding transverse spin currents. Figure 2b shows the energy dependence of γ_S for different values of the staggered perturbation s in the system of Fig. 2a. For increasing values of s the spin skew parameter γ_S decreases and eventually vanishes for large s values. In Fig. 2c we show the effect of s on a sample of randomly sized impurities. We notice that the SHE is robust to impurity size disorder, but it is *not* to staggered potential perturbations; γ_S decreases with increasing values of s , eventually vanishing for all Fermi energies. It is also interesting that the presence of s leads a non-zero valley skewness, γ_V , which would then result in a valley Hall effect, accumulating carriers from different valleys to different edges of the sample. Figure 2d shows the dependence of γ_V on energy and s strength, for a random impurity configuration, reflecting a relatively large value of γ_V for sizable s , while γ_S is much smaller. At high values of s , however, the resonance conditions are offset and both γ_V and γ_S are small in the energy range shown.

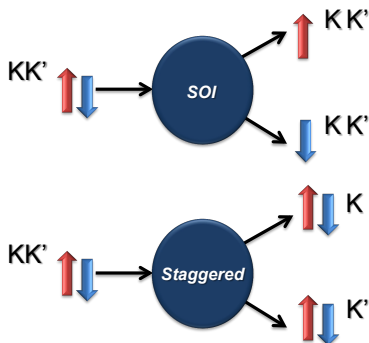


FIG. 3. Schematic representation of spin and valley skew scattering processes due to different perturbations. SOI perturbations act as a spin splitter while leaving the valleys unaffected. The skew character of the scattering remains unaffected in the presence of $V_{\mathcal{T}_1}$. In contrast, the presence perturbations that belong to $V_{\mathcal{T},J}$ and do not commute with \mathcal{T}_1 , such as the staggered potential s , result in valley skewness. In this case the perturbation acts as a valley splitter, while leaving the spin unaffected. In the presence of a staggered potential and SOIs, spin skewness will be reduced, depending on the strength of the staggered effects.

We emphasize that SHE appears and it is enhanced close to the resonant scattering regime,¹⁰ due to the presence of centrosymmetric impurities that enhance SOIs (and produce also a local potential shift). This effect is robust to impurity size and potential disorder,¹⁰ as well as to perturbations that lead to valley mixing in the form $t\mathcal{B}e^{i\Gamma^S\phi}$. Notice also that close to resonance, both the spin and valley Hall effects are enhanced, but become negligible far away from resonance, as is the case for $s/\Delta_{SO} = 80$ in Fig. 2c and d. The competition between these two effects can be schematically illustrated as in Fig. 3: the SHE generated by skew scattering is not robust to a staggered potential, as this leads to a non-zero valley skewness. The latter reduces spin accumulation on the sample edges, while enhancing the valley contrast.

III. DISCUSSION

In light of our results and examination of symmetry breaking effects, let us consider recent experimental results on decorated graphene.

In the experiments by Monteverde *et al.*,³⁶ graphene was deposited on SiO_2 , and a ratio of transport to elastic times $\xi \approx 1.8$ was observed. The lowest carrier concentration for which ξ is reported corresponds to $E \approx 100$ meV (see their Fig. 3). As ξ did not display a sharp drop below the value of 2 until the experimental minimum E considered, we can safely consider that the value of any Rashba SOI is lower than ≈ 200 meV, if present.⁴⁵ [It is interesting to notice that sample A in their Fig. 3 exhibits a drop in the value of ξ for both polarities near the minimum carrier density, suggesting the presence of Rashba

SOI in that sample.] We can also neglect the intrinsic SOI in pristine graphene,⁴² and it being unlikely enhanced by the SiO_2 substrate.⁴³ However, the effects of substrate and impurities are more likely to be symmetry breaking, with a staggered s , and/or hopping modulation t , character. Assuming this to be the case, and comparing with the results of Fig. 1b, we estimate the value of Δ/v (with $\Delta = \sqrt{t^2 + s^2}$) to be $\Delta/v \approx 1/7$, or $\Delta \approx 300$ meV – not an unreasonable estimate of the staggered perturbation strength.

In the experiments by Marchenko *et al.*,¹⁶ Rashba interaction was enhanced through the intercalation of gold atoms between graphene and the Ni substrate. The value of the Rashba interaction was found to depend on the detailed position of the gold atoms with respect to the graphene sample. For samples exhibiting a Rashba interaction of ~ 70 meV, gold atoms were located in the center of the hexagon; for ~ 60 meV, the gold atoms were in the center of non consecutive hexagons; and for ~ 7 meV, the gold atoms were on top of carbon locations. Each of these arrangement can be seen to generate different symmetry breaking terms, in addition to the enhanced SOI. In the case of hexagon-centered gold atoms one expects the perturbation to be dominated by t and v , as these terms possess the symmetries of this specific arrangement. In the cases of 60 and 7meV, one can expect the symmetry breaking to be described by $\{t, s, v\}$ and $\{s, v\}$, respectively. In those cases, the detection and quantification of the Rashba SOI based on transport and elastic times not only allows one to quantify the strength of the Rashba interaction but also to obtain an estimate of the additional parameters of the Hamiltonian (see Fig. 1b).

For example, in the case of a Rashba interaction $\lambda_R = 20$ meV, we notice a sharp drop in the ratio ξ_{SO} for a Fermi energy around this value (indicated by a dashed vertical line) in Fig. 1b. For values of energy larger than 20meV, the ratio displays a nearly constant value, slightly shifted down from the value of 2 (as indicated by horizontal dashed lines in Fig. 1b), with an asymptotic value dependent on the value of Δ/v .

The decoration of graphene with heavy adatoms positioned at the center of hexagons leads to the enhancement of intrinsic SOI.⁴³ The detection and quantification of this interaction through transport measurements becomes masked by symmetry breaking effects, as shown in Fig. 1c. This would lead to overestimation of Δ_{SO} from measurements of ξ_{SO} with varying Fermi energy. This suggests that different measurements, such as SHE should be used in conjunction in order to fully characterize the role of the adatom perturbation.

Skew scattering and the resulting SHE represents an alternative method of quantification of SOIs. The physisorption of nanoparticles on the surface of graphene may be expected to produce a potential shift v and enhanced SOIs with no additional symmetry breaking effects, given their large size when compared to the graphene lattice constant, leading to more accurate quantification of the SOIs.¹¹ Intrinsic SOI enhanced by heavy

adatoms,⁴³ may be characterized through this method. One can expect staggered effects to be weak in these samples, $s \ll \Delta_{SO}$, so that skew scattering would be an important contribution to the SHE.

Our results are also in general agreement with the theoretical analysis by Pachoud *et al.*,⁴⁰ who examine the different low-energy perturbations arising from different adatom locations on the graphene lattice. They notice that the Hall effects produced from hexagon centered or on-top adatoms are of different character. For the hexagon centered position they expect a pure spin Hall effect, in agreement with the symmetry constraints presented in our work. Moreover, for on-top positions it was suggested that if the adatom number of on-*A* and on-*B* types is different, a Hall effect may be observed. This is in agreement with our results for the staggered potential perturbation and the corresponding appearance of a valley Hall effect, which could eventually yield a charge Hall effect for valley polarized currents.

Finally, in hydrogenated samples, where the Rashba interaction is enhanced due to sp^3 deformations,^{9,58} the non-local resistance was seen to be independent of carrier concentration. This suggested that skew scattering was negligible, and the appearance of SHE was attributed to the side-jump mechanism.⁹ The weak contribution of the skew scattering in this kind of sample, however, may also be due to the presence of strong symmetry breaking effects that reduce the conditions for the appearance of SHE, such as a strong staggered perturbation, $s \gg \lambda_R$. This regime would result in a negligible spin skew parameter, as shown in Fig. 2c, due to the dominance of the valley skewness. The persistence of SHE would further suggest that side jump effects are robust to this kind of perturbations, and/or that the phenomenon observed should consider the role of valley skewness in the non local resistance. It would be interesting to carry out a detailed study of this issue in the future.

IV. CONCLUSIONS

We have studied how symmetry breaking effects lead to the appearance of backscattering in graphene, which is reflected among other things on the deviation of the transport to elastic time ratio ξ from its ideal value of 2 at low carrier concentrations. We have also considered that perturbations introduced by adatoms in graphene lead to the enhancement of Rashba-like interactions, in addition to various symmetry breaking effects. In many situations, we find it is possible to detect and separately quantify the SOI and the symmetry breaking amplitudes through measurements of the ratio of transport and energy relaxation times, ξ , as function of carrier concentration. This separability of contributions becomes a challenging task if the SOI enhancement has an intrinsic character, however. In that case, the dependence of ξ on carrier concentration for SOI and symmetry breaking interactions is quite similar, obstructing the extraction

of each effect independently. Finally, we discussed that nonzero spin and/or valley skew parameters, γ_S and γ_V , are expected for certain adatoms. This allows the detection of both Rashba and intrinsic SOIs in the presence of valley mixing effects, even when the transport times ratio may not give definitive answers. For adatoms that enhance SOIs and break sublattice symmetry, we find a reduction of γ_S , which vanishes in systems where the staggered perturbation is larger than the SOI amplitude. As a consequence, the SOI strength would be masked by sublattice symmetry breaking, and the appearance of a valley Hall effect.

ACKNOWLEDGMENTS

We thank N. Sandler and C. Lewenkopf for helpful discussions. MMA is grateful to the 2014 Les Houches Summer School *Topological Aspects of Condensed Matter Physics*, for the welcoming and enlightening environment. This work was supported in part by NSF CIAM/MWN grant DMR-1108285.

Appendix A: Spinless scattering matrix

In the presence of the $V_{T,J,h}$ interactions the operator $\mathcal{T}_1 = ie^{-i\gamma^5\phi}\gamma^5\alpha_2\mathcal{C}$ and time reversal operator $\mathcal{T} = \beta\gamma^5\alpha_1\mathcal{C}$, where \mathcal{C} is the complex conjugation operator, commute with the total Hamiltonian. In addition, $\mathcal{T}_1^2 = -1$, $\mathcal{T}^2 = 1$, $\{\mathcal{T}_1, J_z\} = \{\mathcal{T}, J_z\} = 0$, $[\mathcal{T}_1, \hat{h}] = 0$, $\{\mathcal{T}, \hat{h}\} = 0$, which allows one to choose the states j and $-j$, such that $\mathcal{T}_1\psi_{\pm,j} = \pm(-1)^j\psi_{\pm,-j}$ and $\mathcal{T}\psi_{\pm,j} = \mp(-1)^{j+\frac{1}{2}}\psi_{\mp,-j}$. Note that in cylindrical coordinates one can explicitly write eigenstates that explicitly satisfy these relations, such as $\psi_j = (J_{j-1/2}, iJ_{j+1/2}e^{i\theta}, J_{j-1/2}, -iJ_{j+1/2}e^{i\theta})^T e^{i(j-\frac{1}{2})\theta}$, for $E > 0$, and where $J_l(kr)$ are Bessel functions.⁴⁵

In order to study the scattering problem, the incoming and outgoing states are eigenstates of the free Hamiltonian, $H_0\psi = E\psi$. These eigenstates can be represented with the help of the (helicity) projection operators $P_{\pm} = (1 \pm \gamma^5)/2$, so that a general eigenstate of the Hamiltonian can be written as

$$\psi = P_+\psi + P_-\psi \quad (\text{A1})$$

with $[\hat{h}, P_{\pm}] = 0$ and $\hat{h}(P_{\pm}\psi) = \pm P_{\pm}\psi$. In addition, for a partial wave component we have

$$\begin{aligned} \mathcal{T}_1\psi_j &= \mathcal{T}_1P_+\psi_j + \mathcal{T}_1P_-\psi_j \\ &= (-1)^j(P_+ - P_-)\psi_{-j} \\ &= (-1)^j\gamma^5\psi_{-j}. \end{aligned} \quad (\text{A2})$$

Similarly, for the operator \mathcal{T} , one gets

$$\mathcal{T}\psi_j = (-1)^{j+\frac{1}{2}}\gamma^5\psi_{-j}. \quad (\text{A3})$$

The scattering of a single partial wave j can be written in terms of incoming ψ_j^{in} and outgoing ψ_j^{out} radial eigenstates of the free Hamiltonian,

$$\psi_j = \psi_j^{in} + S_j \psi_j^{out}, \quad (\text{A4})$$

where,

$$S_j = \begin{pmatrix} \hat{S}_{++ ,j} & \hat{S}_{+- ,j} \\ \hat{S}_{-+ ,j} & \hat{S}_{-- ,j} \end{pmatrix}, \quad (\text{A5})$$

$$\hat{S}_j = S_{\tau\tau',j} \sigma_0.$$

Applying the operator \mathcal{T}_1 to the partial wave component ψ_j and using A2 we have

$$\mathcal{T}_1 \psi_j = \mathcal{T}_1 \psi_j^{in} + \mathcal{T}_1 S_j \mathcal{T}_1^{-1} \mathcal{T}_1 \psi_j^{out} \quad (\text{A6})$$

or

$$\psi_{-j} = \psi_{-j}^{out} + \gamma^5 \mathcal{T}_1 S_j \mathcal{T}_1^{-1} \gamma^5 \psi_{-j}^{in}. \quad (\text{A7})$$

Since the S matrix takes a block diagonal form, unitarity $SS^\dagger = 1$, requires $S_j S_j^\dagger = 1$. Comparison with the $-j$ wave component,

$$\psi_{-j} = \psi_{-j}^{in} + S_{-j} \psi_{-j}^{out}, \quad (\text{A8})$$

results in the following condition for S_j ,

$$\gamma^5 \mathcal{T}_1 S_j \mathcal{T}_1^{-1} \gamma^5 = S_{-j}^\dagger, \quad (\text{A9})$$

or equivalently,

$$\begin{pmatrix} \hat{S}_{++ ,j} & -\hat{S}_{+- ,j} e^{2i\phi} \\ -\hat{S}_{-+ ,j} e^{-2i\phi} & \hat{S}_{-- ,j} \end{pmatrix} = \begin{pmatrix} \hat{S}_{++ , -j} & \hat{S}_{-+ , -j} \\ \hat{S}_{+- , -j} & \hat{S}_{-- , -j} \end{pmatrix}. \quad (\text{A10})$$

Similarly, symmetries under \mathcal{T} result in

$$\gamma^5 \mathcal{T} S_j \mathcal{T}^{-1} \gamma^5 = S_{-j}^\dagger, \quad (\text{A11})$$

or

$$\begin{pmatrix} \hat{S}_{-- ,j} & -\hat{S}_{-+ ,j} \\ -\hat{S}_{+- ,j} & \hat{S}_{++ ,j} \end{pmatrix} = \begin{pmatrix} S_{++ , -j} & S_{-+ , -j} \\ S_{+- , -j} & S_{-- , -j} \end{pmatrix}, \quad (\text{A12})$$

with the resulting relations

$$S_{\tau\tau ,j} = S_{\tau\tau , -j} = S_{\bar{\tau}\bar{\tau} , -j} = S_{\bar{\tau}\bar{\tau} , j}, \quad (\text{A13})$$

$$S_{\tau\bar{\tau} ,j} = -S_{\bar{\tau}\tau , -j} e^{-2i\tau\phi} = S_{\bar{\tau}\tau ,j} e^{-2i\tau\phi} = -S_{\tau\bar{\tau} , -j},$$

where $\bar{\tau} = -\tau$.

Appendix B: Spinless cross sections

The amplitudes and corresponding cross sections can be obtained by direct comparison of the far field forms of the incoming and scattered waves in Eq. A4. For an incoming wave front along the x -axis, one can write

$$\psi = e^{ikr \cos \theta} \phi_{in} + \sum_j \hat{f}_j e^{ij\theta} \frac{e^{ikr}}{\sqrt{r}} \phi_{in}, \quad (\text{B1})$$

where \hat{f}_j is a matrix containing the different scattering amplitudes for each angular momentum channel j , and ϕ_{in} is a spinor representing the different incoming valley weights. The scattering amplitudes in each j -block are given by⁵⁹

$$\hat{f}_j = \frac{e^{-i\pi/4}}{\sqrt{2\pi k}} \begin{pmatrix} (\hat{S}_{++ ,j} - 1) & -i\hat{S}_{+- ,j} \\ i\hat{S}_{-+ ,j} & (\hat{S}_{-- ,j} - 1) \end{pmatrix} \quad (\text{B2})$$

and related to different cross sections by

$$\sigma_{\tau\tau'}(\theta) = \frac{1}{2\pi k} \left| \sum_{j=-\infty}^{\infty} f_{\tau\tau',j} e^{ij\theta} \right|^2,$$

$$\sigma_{t,\tau\tau'} = \int_{-\pi}^{\pi} \sigma_{\tau\tau'}(\theta) d\theta = \frac{1}{k} \sum_{j=-\infty}^{\infty} |f_{\tau\tau',j}|^2,$$

$$\sigma_{tr,\tau\tau'} = \int_{-\pi}^{\pi} \sigma_{\tau\tau'}(\theta) (1 - \cos \theta) d\theta = \sigma_{t,\tau\tau'} - \frac{1}{k} \sum_{j=-\infty}^{\infty} \text{Re}(f_{\tau\tau',j} f_{\tau\tau',j+1}^*),$$

$$\sigma_{sk,\tau\tau'} = \int_{-\pi}^{\pi} \sigma_{\tau\tau'}(\theta) \sin \theta d\theta = \frac{1}{k} \sum_{j=-\infty}^{\infty} \text{Im}(f_{\tau\tau',j} f_{\tau\tau',j+1}^*), \quad (\text{B3})$$

where j is a half integer in all the sums. Here, $\sigma_{\tau\tau'}(\theta)$ is the differential cross section, while $\sigma_{t,\tau\tau'}$ is the total, $\sigma_{tr,\tau\tau'}$ is the transport, and $\sigma_{sk,\tau\tau'}$ is the skew cross section, all with valley preserving ($\tau = \tau'$) and valley flipping ($\tau \neq \tau'$) channels. We similarly define the valley averaged quantities,

$$\begin{aligned}\sigma(\theta) &= \sum_{\tau\tau'} \sigma_{\tau\tau'}(\theta), \\ \sigma_t &= \sum_{\tau\tau'} \sigma_{t,\tau\tau'}, \\ \sigma_{tr} &= \sum_{\tau\tau'} \sigma_{tr,\tau\tau'}, \\ \sigma_{sk} &= \sum_{\tau\tau'} \sigma_{sk,\tau\tau'}.\end{aligned}\quad (\text{B4})$$

The presence of $V_{T,J,h}$ perturbations ensures that the set of relations in Eq. A13 are satisfied, so that

$$\begin{aligned}f_{\tau\tau,j} &= f_{\tau\tau,-j} = f_{\bar{\tau}\bar{\tau},-j} = f_{\bar{\tau}\bar{\tau},j}, \\ f_{\tau\bar{\tau},j} &= -f_{\bar{\tau}\tau,-j}e^{-2i\tau\phi} = f_{\bar{\tau}\tau,j}e^{-2i\tau\phi} = -f_{\tau\bar{\tau},-j}.\end{aligned}\quad (\text{B5})$$

Consequently,

$$\begin{aligned}\sum_{j=-\infty}^{\infty} f_{\tau\tau,j} e^{ij\theta} &= \sum_{j \geq \frac{1}{2}} 2f_{\tau\tau,j} \cos(j\theta), \\ \sum_{j=-\infty}^{\infty} f_{\tau\bar{\tau},j} e^{ij\theta} &= \sum_{j \geq \frac{1}{2}} 2if_{\tau\bar{\tau},j} \sin(j\theta),\end{aligned}\quad (\text{B6})$$

which results in Eq. 36 in the text. Notice also that

$$\begin{aligned}\sum_{j=-\infty}^{\infty} f_{\tau\tau,j} f_{\tau\tau,j+1}^* &= |f_{\tau\tau,\frac{1}{2}}|^2 + \sum_{j \geq \frac{1}{2}} 2\text{Re}(f_{\tau\tau,j} f_{\tau\tau,j+1}^*), \\ \sum_{j=-\infty}^{\infty} f_{\tau\bar{\tau},j} f_{\tau\bar{\tau},j+1}^* &= -|f_{\tau\bar{\tau},\frac{1}{2}}|^2 + \sum_{j \geq \frac{1}{2}} 2\text{Re}(f_{\tau\bar{\tau},j} f_{\tau\bar{\tau},j+1}^*),\end{aligned}\quad (\text{B7})$$

which results in

$$\begin{aligned}\sum_{j=-\infty}^{\infty} \text{Im}(f_{\tau\tau,j} f_{\tau\tau,j+1}^*) &= 0, \\ \sum_{j=-\infty}^{\infty} \text{Im}(f_{\tau\bar{\tau},j} f_{\tau\bar{\tau},j+1}^*) &= 0.\end{aligned}\quad (\text{B8})$$

Now, when $kR \ll 1$, the only scattering channels with non vanishing amplitudes are $j = \pm\frac{1}{2}$, and the ratio of transport to elastic times becomes

$$\xi = \frac{\tau_{tr}}{\tau_e} = \frac{\sigma_t}{\sigma_{tr}} = \frac{\sum_{\tau\tau'} \sigma_{t,\tau\tau'}}{\sum_{\tau\tau'} \sigma_{tr,\tau\tau'}}, \quad (\text{B9})$$

where,

$$\begin{aligned}\sigma_{t,\tau\tau} &\approx \frac{2}{k} |f_{\tau\tau,\frac{1}{2}}|^2 = 2\sigma_{tr,\tau\tau}, \\ \sigma_{t,\tau\bar{\tau}} &\approx \frac{2}{k} |f_{\tau\bar{\tau},\frac{1}{2}}|^2, \\ \sigma_{tr,\tau\bar{\tau}} &\approx \frac{3}{k} |f_{\tau\bar{\tau},\frac{1}{2}}|^2, \\ \sigma_{sk,\tau\tau} &= \sigma_{sk,\tau\bar{\tau}} = 0.\end{aligned}\quad (\text{B10})$$

This yields

$$\xi = \frac{\sigma_t}{\sigma_{tr}} = \frac{2\left(|f_{++,\frac{1}{2}}|^2 + |f_{+-,\frac{1}{2}}|^2\right)}{|f_{++,\frac{1}{2}}|^2 + 3|f_{+-,\frac{1}{2}}|^2}, \quad (\text{B11})$$

which appears as Eq. 42 in the text.

1. $V_{T,J}$ perturbations

In the presence of interactions that belong to the set $V_{T,J}$, the conditions on the scattering matrix elements are

those resulting only from time reversal symmetry, such that they are reduced to those in A12,

$$\begin{aligned}S_{\tau\tau,j} &= S_{\bar{\tau}\bar{\tau},-j}, \\ S_{\tau\bar{\tau},j} &= -S_{\tau\bar{\tau},-j}, \\ S_{\tau\bar{\tau},j} &= -S_{\bar{\tau}\tau,-j},\end{aligned}\quad (\text{B12})$$

and correspondingly,

$$\begin{aligned}f_{\tau\tau,j} &= f_{\bar{\tau}\bar{\tau},-j}, \\ f_{\tau\bar{\tau},j} &= -f_{\tau\bar{\tau},-j}, \\ f_{\tau\bar{\tau},j} &= -f_{\bar{\tau}\tau,-j}.\end{aligned}\quad (\text{B13})$$

These relations cannot guarantee B7 and B8, so that for example $\sum_{j=-\infty}^{\infty} \text{Im}(f_{\tau\tau,j} f_{\tau\tau,j+1}^*)$ is not identically zero by symmetry; instead, its value depends on the details of the perturbations in the Hamiltonian. As a consequence, one can write

$$\begin{aligned}\sigma_{t,\tau\tau} &= \sigma_{t,\bar{\tau}\bar{\tau}}, \\ \sigma_{tr,\tau\tau} &= \sigma_{tr,\bar{\tau}\bar{\tau}}, \\ \sigma_{sk,\tau\tau} &= -\sigma_{sk,\bar{\tau}\bar{\tau}}, \\ \sigma_{t,\tau\bar{\tau}} &= \sigma_{t,\bar{\tau}\tau}, \\ \sigma_{tr,\tau\bar{\tau}} &= \sigma_{tr,\bar{\tau}\tau}, \\ \sigma_{sk,\tau\bar{\tau}} &= \sigma_{sk,\bar{\tau}\tau} = 0.\end{aligned}\quad (\text{B14})$$

The skew parameter is defined as

$$\gamma = \frac{\sum_{\tau\tau'} \sigma_{sk,\tau\tau'}}{\sum_{\tau\tau'} \sigma_{tr,\tau\tau'}}. \quad (\text{B15})$$

The relations $\sigma_{sk,\tau\tau} \neq 0$ and $\sigma_{sk,\tau\bar{\tau}} = 0$ indicate the presence of transverse valley currents, which would result

in the valley Hall effect. These currents are related to the valley skew parameter at zero temperatures by

$$\gamma_V = \frac{j_{VH}}{j_x} = \frac{1}{2}(\gamma_K - \gamma_{K'}), \quad (\text{B16})$$

where

$$\gamma_\tau = \frac{\sum_{\tau'} \sigma_{sk,\tau'\tau}}{\sum_{\tau'} \sigma_{tr,\tau'\tau}}. \quad (\text{B17})$$

Moreover, for valley-polarized incident flux, $\gamma = \gamma_V \neq 0$ in general. This would in principle produce a charge Hall voltage, due to the accumulation of carriers of a given valley at one edge of the sample.

This effect is absent in the usual valley unpolarized currents, as $\sigma_{sk,\tau\tau} = -\sigma_{sk,\bar{\tau}\bar{\tau}}$, $\sigma_{sk,\tau\tau'} = 0$ and $\gamma = 0$, so that there is no net charge on the edges and no Hall effect is produced.

In the case of $kR \ll 1$, we notice from Eq. B13 that the amplitudes of the dominant two j -channels in this regime ($j = \pm \frac{1}{2}$) are not all related by symmetry, which results in $1 < \xi < 2$, and dependent on the specific parameters of the Hamiltonian. When $\Delta/|E - v| \rightarrow 0$ (ultrarelativistic regime), one recovers $\xi \rightarrow 2$, while $\xi \rightarrow 1$ as $\Delta/|E - v| \rightarrow 1$.^{45,55}

Appendix C: Scattering matrix and spin-orbit interactions

In the presence of spin-orbit interactions that commute with the total angular momentum, $V_{T,J}^{SO}$, and spin independent interactions that belong to $V_{\mathcal{T}_1}$ (see Sec. II B), both $\mathcal{T}_1 = e^{-i\Gamma^5 \phi} \Gamma^5 \mathcal{A}_2 S_2 \mathcal{C}$ and $\mathcal{T} = i\mathcal{B} \Gamma^5 \mathcal{A}_1 S_2 \mathcal{C}$ operators commute with $H = H_0 + V_{\mathcal{T}_1}$, and allows us relate the states with j and $-j$; here one can write

$\psi_j = (J_{j-1} e^{-i\theta}, iJ_j, J_{j-1} e^{-i\theta}, -iJ_j, J_j, iJ_{j+1} e^{i\theta}, J_j, -iJ_{j+1} e^{i\theta})^T e^{ij\theta}$, and where $J_l(kr)$ are Bessel functions.⁴⁵

In the presence of SO interactions, an incident state could be projected into valley and spin subspaces with the aid of the corresponding projection operators, given by $P_\pm = (1 \pm \Gamma^5)/2$ and $P_{\uparrow/\downarrow} = (1 \pm S_z)/2$. A general eigenstate of H_0 can then be written as

$$\psi = P_+(P_\uparrow + P_\downarrow)\psi + P_-(P_\uparrow + P_\downarrow)\psi. \quad (\text{C1})$$

The partial wave components can be chosen to satisfy $\mathcal{T}_1 P_\pm P_s \psi_j = \pm (-1)^j P_\pm P_{\bar{s}} \psi_{-j}$ and $\mathcal{T} P_\pm P_s \psi_j = \mp (-1)^{j+\frac{1}{2}} P_\mp P_s \psi_{-j}$. Consequently

$$\begin{aligned} \mathcal{T}_1 \psi_j &= (-1)^j (P_+(P_\uparrow + P_\downarrow)\psi_{-j} - P_-(P_\uparrow + P_\downarrow)\psi_{-j}), \\ &= (-1)^j \Gamma^5 \psi_{-j}, \end{aligned} \quad (\text{C2})$$

and

$$\begin{aligned} \mathcal{T} \psi_j &= (-1)^{j+\frac{1}{2}} (P_+(P_\uparrow + P_\downarrow)\psi_{-j} - P_-(P_\uparrow + P_\downarrow)\psi_{-j}), \\ &= (-1)^{j+\frac{1}{2}} \Gamma^5 \psi_{-j}. \end{aligned} \quad (\text{C3})$$

As before, the incoming and outgoing partial waves describing the scattering problem can be written as

$$\psi_j = \psi_j^{in} + S_j \psi_j^{out}. \quad (\text{C4})$$

In this case, the scattering matrix can be written in terms of 4×4 , S_j -blocks, with elements $\hat{S}_{\tau\tau',ss',j}$. By applying the operator \mathcal{T}_1 to Eq. C4, we get

$$\Gamma^5 \mathcal{T}_1 S_j \mathcal{T}_1^{-1} \Gamma^5 = S_{-j}^\dagger, \quad (\text{C5})$$

and by applying \mathcal{T} we get

$$\Gamma^5 \mathcal{T} S_j \mathcal{T}^{-1} \Gamma^5 = S_{-j}^\dagger. \quad (\text{C6})$$

From these conditions and unitarity of S_j we have,

$$\begin{aligned} S_{\tau\tau,ss,j} &= S_{\bar{\tau}\bar{\tau},\bar{s}\bar{s},-j} = S_{\tau\tau,\bar{s}\bar{s},-j} \\ S_{\tau\bar{\tau},ss,j} &= -S_{\tau\bar{\tau},\bar{s}\bar{s},-j} = -S_{\bar{\tau}\bar{\tau},\bar{s}\bar{s},-j} e^{2i\tau\phi} \\ S_{\tau\bar{\tau},s\bar{s},j} &= S_{\tau\bar{\tau},s\bar{s},-j} = -S_{\bar{\tau}\bar{\tau},\bar{s}\bar{s},-j} = -S_{\bar{\tau}\bar{\tau},s\bar{s},-j} e^{2i\tau\phi} = -S_{\tau\tau,\bar{s}\bar{s},-j} e^{2i\tau\phi} \\ S_{\tau\tau,s\bar{s},j} &= S_{\tau\tau,s\bar{s},-j} = -S_{\bar{\tau}\bar{\tau},\bar{s}\bar{s},-j} e^{2i\tau\phi}. \end{aligned} \quad (\text{C7})$$

The scattering amplitudes are given by

$$\hat{f}_j(\theta) = \frac{e^{-i\pi/4}}{\sqrt{2\pi k}} \begin{pmatrix} (\hat{S}_{++\uparrow\uparrow,j} - 1) & -i\hat{S}_{+-,\uparrow\uparrow,j} & -i\hat{S}_{++,\uparrow\downarrow,j} & -\hat{S}_{+-,\uparrow\downarrow,j} \\ i\hat{S}_{-+,\uparrow\uparrow,j} & (\hat{S}_{--\uparrow\uparrow,j} - 1) & \hat{S}_{-+,\uparrow\downarrow,j} & -i\hat{S}_{--,\uparrow\downarrow,j} \\ i\hat{S}_{++,\downarrow\uparrow,j} & \hat{S}_{+-,\downarrow\uparrow,j} & (\hat{S}_{++\downarrow\downarrow,j} - 1) & -i\hat{S}_{+-,\downarrow\downarrow,j} \\ -\hat{S}_{-+,\downarrow\uparrow,j} & i\hat{S}_{--,\downarrow\uparrow,j} & i\hat{S}_{-+,\downarrow\downarrow,j} & (\hat{S}_{--\downarrow\downarrow,j} - 1) \end{pmatrix}, \quad (\text{C8})$$

and the different cross sections

$$\begin{aligned}
\sigma_{\tau\tau',ss'}(\theta) &= \frac{1}{2\pi k} \left| \sum_{j=-\infty}^{\infty} f_{j,\tau\tau',ss'} e^{ij\theta} \right|^2, \\
\sigma_{t,\tau\tau',ss'} &= \frac{1}{k} \sum_{j=-\infty}^{\infty} |f_{j,\tau\tau',ss'}|^2, \\
\sigma_{tr,\tau\tau',ss'} &= \sigma_{t,\tau\tau',ss'} - \frac{1}{k} \sum_{j=-\infty}^{\infty} \text{Re}(f_{j,\tau\tau',ss'} f_{j+1\tau\tau',ss'}^*), \\
\sigma_{sk,\tau\tau',ss'} &= \frac{1}{k} \sum_{j=-\infty}^{\infty} \text{Im}(f_{j,\tau\tau',ss'} f_{j+1\tau\tau',ss'}^*).
\end{aligned} \tag{C9}$$

These help define the ratio of transport to elastic times in the presence of SOI,

$$\xi_{SO} = \frac{\sum_{\tau\tau',ss'} \sigma_{t,\tau\tau',ss'}}{\sum_{\tau\tau',ss'} \sigma_{tr,\tau\tau',ss'}}, \tag{C10}$$

and skew parameter

$$\begin{aligned}
\gamma_S &= \frac{1}{2}(\gamma_{\uparrow} - \gamma_{\downarrow}), \\
\gamma_s &= \frac{\sum_{\tau,\tau',s'} \sigma_{sk,\tau\tau',s's}}{\sum_{\tau,\tau',s'} \sigma_{tr,\tau\tau',s's}}.
\end{aligned} \tag{C11}$$

For interactions commuting with \mathcal{T} and \mathcal{T}_1 , we have the relations

$$\begin{aligned}
\sum_{j=-\infty}^{\infty} f_{\tau\tau,ss,j} f_{\tau\tau,ss,j+1}^* &= \left(\sum_{j=-\infty}^{\infty} f_{\bar{\tau}\bar{\tau},\bar{s}\bar{s},j} f_{\bar{\tau}\bar{\tau},\bar{s}\bar{s},j+1}^* \right)^* = \left(\sum_{j=-\infty}^{\infty} f_{\tau\tau,\bar{s}\bar{s},j} f_{\tau\tau,\bar{s}\bar{s},j+1}^* \right)^* = \sum_{j=-\infty}^{\infty} f_{\bar{\tau}\bar{\tau},ss,j} f_{\bar{\tau}\bar{\tau},ss,j+1}^*, \\
\sum_{j=-\infty}^{\infty} f_{\tau\bar{\tau},ss,j} f_{\tau\bar{\tau},ss,j+1}^* &= \sum_{j=-\infty}^{\infty} f_{\bar{\tau}\tau,ss,j} f_{\bar{\tau}\tau,ss,j+1}^* = \left(\sum_{j=-\infty}^{\infty} f_{\bar{\tau}\tau,\bar{s}\bar{s},j} f_{\bar{\tau}\tau,\bar{s}\bar{s},j+1}^* \right)^* = \left(\sum_{j=-\infty}^{\infty} f_{\tau\bar{\tau},\bar{s}\bar{s},j} f_{\tau\bar{\tau},\bar{s}\bar{s},j+1}^* \right)^*, \\
\sum_{j=-\infty}^{\infty} \text{Im}(f_{\tau\tau',s\bar{s},j} f_{\tau\tau',s\bar{s},j+1}^*) &= \sum_{j=-\infty}^{\infty} \text{Im}(f_{\tau\tau',\bar{s}s,j} f_{\tau\tau',\bar{s}s,j+1}^*) = 0,
\end{aligned} \tag{C12}$$

and consequently,

$$\begin{aligned}
\sigma_{t,\tau\tau,ss} &= \sigma_{t,\tau\tau,\bar{s}\bar{s}} = \sigma_{t,\bar{\tau}\bar{\tau},\bar{s}\bar{s}} = \sigma_{t,\bar{\tau}\bar{\tau},ss}, \\
\sigma_{tr,\tau\tau,ss} &= \sigma_{tr,\tau\tau,\bar{s}\bar{s}} = \sigma_{tr,\bar{\tau}\bar{\tau},\bar{s}\bar{s}} = \sigma_{tr,\bar{\tau}\bar{\tau},ss}, \\
\sigma_{sk,\tau\tau,ss} &= -\sigma_{sk,\tau\tau,\bar{s}\bar{s}} = -\sigma_{sk,\bar{\tau}\bar{\tau},\bar{s}\bar{s}} = \sigma_{sk,\bar{\tau}\bar{\tau},ss}, \\
\sigma_{t,\tau\bar{\tau},ss} &= \sigma_{t,\bar{\tau}\tau,ss} = \sigma_{t,\bar{\tau}\tau,\bar{s}\bar{s}} = \sigma_{t,\tau\bar{\tau},\bar{s}\bar{s}}, \\
\sigma_{tr,\tau\bar{\tau},ss} &= \sigma_{tr,\bar{\tau}\tau,ss} = \sigma_{tr,\bar{\tau}\tau,\bar{s}\bar{s}} = \sigma_{tr,\tau\bar{\tau},\bar{s}\bar{s}}, \\
\sigma_{sk,\tau\bar{\tau},ss} &= \sigma_{sk,\bar{\tau}\tau,ss} = -\sigma_{sk,\bar{\tau}\tau,\bar{s}\bar{s}} = -\sigma_{sk,\tau\bar{\tau},\bar{s}\bar{s}}, \\
\sigma_{t,\tau\tau',s\bar{s}} &= \sigma_{t,\tau\tau',\bar{s}s}, \\
\sigma_{tr,\tau\tau',s\bar{s}} &= \sigma_{tr,\tau\tau',\bar{s}s}, \\
\sigma_{sk,\tau\tau',s\bar{s}} &= \sigma_{sk,\tau\tau',\bar{s}s} = 0.
\end{aligned} \tag{C13}$$

This leads to $\gamma_{\uparrow} = -\gamma_{\downarrow}$ and $\gamma_S = \gamma_{\uparrow}$, so that even for a valley and spin unpolarized incident wave, there is

accumulation of different spins on edges of the sample, and the corresponding appearance of the spin Hall effect.

In the presence of SOIs the total angular momentum is an integer ($j \in Z$), as noted before. Then for $kR \ll 1$, there are *three* dominant angular momentum channels in the scattering process, $j = 0, \pm 1$. In the case of resonance, these channels resonate at different energies, leading to a drop of ξ_{SO} towards 1 at these energies, as the scattering process is predominantly caused by only one of the channels for a given spin kind.

In the case where the perturbations present *do not*

commute with \mathcal{T}_1 , instead of C13 we have

$$\begin{aligned}
 \sigma_{t,\tau\tau,ss} &= \sigma_{t,\bar{\tau}\bar{\tau},\bar{s}\bar{s}} , \\
 \sigma_{tr,\tau\tau,ss} &= \sigma_{tr,\bar{\tau}\bar{\tau},\bar{s}\bar{s}} , \\
 \sigma_{sk,\tau\tau,ss} &= -\sigma_{sk,\bar{\tau}\bar{\tau},\bar{s}\bar{s}} , \\
 \sigma_{t,\tau\bar{\tau},ss} &= \sigma_{t,\tau\bar{\tau},\bar{s}\bar{s}} , \\
 \sigma_{tr,\tau\bar{\tau},ss} &= \sigma_{tr,\tau\bar{\tau},\bar{s}\bar{s}} , \\
 \sigma_{sk,\tau\bar{\tau},ss} &= -\sigma_{sk,\tau\bar{\tau},\bar{s}\bar{s}} , \\
 \sigma_{sk,\tau\tau',s\bar{s}} &= \sigma_{sk,\tau\tau',\bar{s}s} = 0 .
 \end{aligned}
 \tag{C14}$$

In this case, γ_S gets reduced from its optimal value, which indicates that $V_{\mathcal{T},J}$ perturbations that do not commute with \mathcal{T}_1 lead to a reduction in the possible SHE: the competition with valley skew scattering (produced by a staggered perturbation, for example) will result in a reduction of the spin imbalance accumulated at the edges of the samples. As such $V_{\mathcal{T},J}$ perturbations increase, γ_S may even become negligible, as $\gamma_{\uparrow} \simeq \gamma_{\downarrow}$ if valley skewness dominates, as schematically represented in Fig. 3.

* asmar@phy.ohio.edu

† ulloa@ohio.edu

- ¹ A. H. Castro Neto, F. Guinea, N. M. R. Peres, K. S. Novoselov, and A. K. Geim, *Rev. Mod. Phys.* **81**, 109 (2009).
- ² C. L. Kane and E. J. Mele, *Phys. Rev. Lett.* **95**, 226801 (2005).
- ³ L. Fu and C. L. Kane, *Phys. Rev. B* **74**, 195312 (2006).
- ⁴ D. Hsieh, D. Qian, L. Wray, Y. Xia, Y. S. Hor, R. J. Cava, and M. Z. Hasan, *Nature* **452**, 970 (2008).
- ⁵ A. P. Schnyder, S. Ryu, A. Furusaki, and A. W. W. Ludwig, *Phys. Rev. B* **78**, 195125 (2008).
- ⁶ M. Z. Hasan and C. L. Kane, *Rev. Mod. Phys.* **82**, 3045 (2010).
- ⁷ X.-L. Qi and S.-C. Zhang, *Rev. Mod. Phys.* **83**, 1057 (2011).
- ⁸ A. H. Castro Neto and F. Guinea, *Phys. Rev. Lett.* **103**, 026804 (2009).
- ⁹ J. Balakrishnan, G. Kok Wai Koon, M. Jaiswal, A. H. Castro Neto, and B. Özyilmaz, *Nat. Phys.* **9**, 284 (2013).
- ¹⁰ A. Ferreira, T. G. Rappoport, M. A. Cazalilla, and A. H. Castro Neto, *Phys. Rev. Lett.* **112**, 066601 (2014).
- ¹¹ J. Balakrishnan, G. K. W. Koon, A. Avsar, Y. Ho, J. H. Lee, M. Jaiswal, S.-J. Baeck, J.-H. Ahn, A. Ferreira, M. A. Cazalilla, A. H. C. Neto, and B. Özyilmaz, *Nat. Commun.* **5** (2014).
- ¹² K. S. Novoselov, D. Jiang, F. Schedin, T. J. Booth, V. V. Khotkevich, S. V. Morozov, and A. K. Geim, *PNAS* **102**, 10451 (2005).
- ¹³ K. S. Novoselov and A. H. C. Neto, *Phys. Scripta* **2012**, 014006 (2012).
- ¹⁴ A. Varykhalov, J. Sánchez-Barriga, A. M. Shikin, C. Biswas, E. Vescovo, A. Rybkin, D. Marchenko, and O. Rader, *Phys. Rev. Lett.* **101**, 157601 (2008).
- ¹⁵ K. Pi, W. Han, K. M. McCreary, A. G. Swartz, Y. Li, and R. K. Kawakami, *Phys. Rev. Lett.* **104**, 187201 (2010).
- ¹⁶ D. Marchenko, A. Varykhalov, M. Scholz, G. Bihlmayer, E. Rashba, A. Rybkin, A. Shikin, and O. Rader, *Nat. Commun.* **3**, 1232 (2012).
- ¹⁷ J. Zhang, C. Triola, and E. Rossi, *Phys. Rev. Lett.* **112**, 096802 (2014).
- ¹⁸ C. R. Woods, L. Britnell, A. Eckmann, R. S. Ma, J. C. Lu, H. M. Guo, X. Lin, G. L. Yu, Y. Cao, R. V. Gorbachev, A. V. Kretinin, J. Park, L. A. Ponomarenko, M. I. Katsnelson, Y. N. Gornostyrev, K. Watanabe, T. Taniguchi, C. Casiraghi, H.-J. Gao, A. K. Geim, and K. S. Novoselov, *Nat. Phys.* **10**, 451 (2014).
- ¹⁹ T. Ando, *J. Phys. Soc. Jap.* **69**, 1757 (2000).
- ²⁰ A. De Martino, R. Egger, K. Hallberg, and C. A. Balseiro, *Phys. Rev. Lett.* **88**, 206402 (2002).
- ²¹ L. Chico, M. P. López-Sancho, and M. C. Muñoz, *Phys. Rev. Lett.* **93**, 176402 (2004).
- ²² D. Huertas-Hernando, F. Guinea, and A. Brataas, *Phys. Rev. B* **74**, 155426 (2006).
- ²³ C.-Y. Hou, C. Chamon, and C. Mudry, *Phys. Rev. Lett.* **98**, 186809 (2007).
- ²⁴ V. Cheianov, V. Fal'ko, O. Syljuasen, and B. Altshuler, *Solid State Comm.* **149**, 1499 (2009).
- ²⁵ J.-S. Jeong, J. Shin, and H.-W. Lee, *Phys. Rev. B* **84**, 195457 (2011).
- ²⁶ T. Iadecola, D. Campbell, C. Chamon, C.-Y. Hou, R. Jackiw, S.-Y. Pi, and S. V. Kusminskiy, *Phys. Rev. Lett.* **110**, 176603 (2013).
- ²⁷ T. Iadecola, T. Neupert, and C. Chamon, *Phys. Rev. B* **89**, 115425 (2014).
- ²⁸ M. I. Katsnelson, K. S. Novoselov, and A. K. Geim, *Nat. Phys.* **2**, 620 (2006).
- ²⁹ F. V. Tikhonenko, A. A. Kozikov, A. K. Savchenko, and R. V. Gorbachev, *Phys. Rev. Lett.* **103**, 226801 (2009).
- ³⁰ I. L. Aleiner and K. B. Efetov, *Phys. Rev. Lett.* **97**, 236801 (2006).
- ³¹ A. F. Morpurgo and F. Guinea, *Phys. Rev. Lett.* **97**, 196804 (2006).
- ³² E. McCann, K. Kechedzhi, V. I. Fal'ko, H. Suzuura, T. Ando, and B. L. Altshuler, *Phys. Rev. Lett.* **97**, 146805 (2006).
- ³³ P. M. Ostrovsky, I. V. Gornyi, and A. D. Mirlin, *Phys. Rev. B* **74**, 235443 (2006).
- ³⁴ J. L. Mañes, F. Guinea, and M. A. H. Vozmediano, *Phys. Rev. B* **75**, 155424 (2007).
- ³⁵ X. Hong, K. Zou, and J. Zhu, *Phys. Rev. B* **80**, 241415 (2009).
- ³⁶ M. Monteverde, C. Ojeda-Aristizabal, R. Weil, K. Benameur, M. Ferrier, S. Guéron, C. Glattli, H. Bouchiat, J. N. Fuchs, and D. L. Maslov, *Phys. Rev. Lett.* **104**, 126801 (2010).
- ³⁷ E. R. Mucciolo and C. H. Lewenkopf, *J. Phys. Condens. Matter* **22**, 273201 (2010).
- ³⁸ E. McCann and V. I. Fal'ko, *Phys. Rev. Lett.* **108**, 166606 (2012).
- ³⁹ F. de Juan, *Phys. Rev. B* **87**, 125419 (2013).
- ⁴⁰ A. Pachoud, A. Ferreira, B. Özyilmaz, and A. H. Castro Neto, *Phys. Rev. B* **90**, 035444 (2014).
- ⁴¹ E. Rashba, *Sov. Phys. Solid State* **2**, 1109 (1960).
- ⁴² H. Min, J. E. Hill, N. A. Sinitsyn, B. R. Sahu, L. Kleinman, and A. H. MacDonald, *Phys. Rev. B* **74**, 165310 (2006).

- ⁴³ C. Weeks, J. Hu, J. Alicea, M. Franz, and R. Wu, *Phys. Rev. X* **1**, 021001 (2011).
- ⁴⁴ Z. Jia, B. Yan, J. Niu, Q. Han, R. Zhu, D. Yu, and X. Wu, *Phys. Rev. B* **91**, 085411 (2015).
- ⁴⁵ M. M. Asmar and S. E. Ulloa, *Phys. Rev. Lett.* **112**, 136602 (2014).
- ⁴⁶ D. Huertas-Hernando, F. Guinea, and A. Brataas, *Phys. Rev. Lett.* **103**, 146801 (2009).
- ⁴⁷ H. Ochoa, A. H. Castro Neto, and F. Guinea, *Phys. Rev. Lett.* **108**, 206808 (2012).
- ⁴⁸ M. M. Asmar and S. E. Ulloa, *Phys. Rev. B* **87**, 075420 (2013).
- ⁴⁹ M. I. Katsnelson, F. Guinea, and A. K. Geim, *Phys. Rev. B* **79**, 195426 (2009).
- ⁵⁰ M. E. Peskin and D. V. Schroeder, *An Introduction To Quantum Field Theory* (Westview Press, 1995).
- ⁵¹ M. Srednicki, *Quantum Field Theory* (Cambridge University Press, New York, 2007).
- ⁵² S. Ryu, C. Mudry, C.-Y. Hou, and C. Chamon, *Phys. Rev. B* **80**, 205319 (2009).
- ⁵³ C. W. J. Beenakker, *Rev. Mod. Phys.* **80**, 1337 (2008).
- ⁵⁴ D. S. Novikov, *Phys. Rev. B* **76**, 245435 (2007).
- ⁵⁵ J. H. Bardarson, M. Titov, and P. W. Brouwer, *Phys. Rev. Lett.* **102**, 226803 (2009).
- ⁵⁶ D. Xiao, W. Yao, and Q. Niu, *Phys. Rev. Lett.* **99**, 236809 (2007).
- ⁵⁷ A. De Martino, A. Hütten, and R. Egger, *Phys. Rev. B* **84**, 155420 (2011).
- ⁵⁸ D. C. Elias, R. R. Nair, T. M. G. Mohiuddin, S. V. Morozov, P. Blake, M. P. Halsall, A. C. Ferrari, D. W. Boukhvalov, M. I. Katsnelson, A. K. Geim, and K. S. Novoselov, *Science* **323**, 610 (2009).
- ⁵⁹ J. J. Sakurai, *Modern Quantum Mechanics* (Addison Wesley, 1993).